Tunnelling and Underground Space Technology 155 (2025) 106137

Contents lists available at ScienceDirect

Tunnelling and Underground Space Technology

journal homepage: www.elsevier.com/locate/tust

Lower and upper bounds for the drained three-dimensional stability of shallow tunnels using the Extended Matsuoka-Nakai yield criterion

A.N. Antão [a,b,*], M. Vicente da Silva [b]

[a] CERIS, Departamento de Engenharia Civil, Faculdade de Ciências e Tecnologia, Universidade NOVA de Lisboa, Campus de Caparica, Caparica, 2829-516, Portugal

[b] Departamento de Engenharia Civil, Faculdade de Ciências e Tecnologia, Universidade NOVA de Lisboa, Campus de Caparica, Caparica, 2829-516, Portugal

ARTICLE INFO

Keywords:
Tunnel stability
Three-dimensional
Extended-matsuoka-nakai criterion
Limit analysis

ABSTRACT

The paper focuses on determining lower and upper approximations of the pressure required on the unlined part of a tunnel's front under drained conditions. This work is carried out within the framework of classic limit analysis. In the last three decades, various approaches have been explored to enhance the understanding of the minimum pressure required for ensuring the stability of the massif during tunnel excavation under drained conditions. Methods for solving this problem are typically categorized as limit equilibrium methods, limit analysis methods, or elasto-plastic stress–strain calculations. However, the failure criterion used has almost invariably been the Mohr–Coulomb criterion. Despite its broad application, this criterion has certain limitations in evaluating the effect of the three principal stresses on the yield of earthy or rocky materials. Over time, alternative failure criteria have been proposed to address this issue, including one developed by Matsuoka and Nakai.

This work applies Limit Analysis theorems to this problem using an extended Matsuoka-Nakai criterion. Besides providing highly accurate stability factors for tunnels using this criterion, the novelty of this study also lies in the comparative analysis of numerical results with experimental data, demonstrating that the Matsuoka-Nakai criterion offers a more accurate model of the experimental data compared to the traditional Mohr–Coulomb approach.

1. Introduction

The stability of tunnels during excavation, especially in soil, poses a significant challenge for their designers. This three-dimensional problem is influenced by various factors, with soil drainage capacity standing out as a fundamental aspect. During the construction stage, the drainage ability dictates whether the conditions are drained or undrained. This paper specifically focuses on drained stability.

Over the past few decades, extensive efforts have been dedicated to studying this issue through numerical, analytical, and experimental approaches. These endeavors aim to enhance our understanding of the complexities involved in ensuring the stability of tunnels during excavation.

In the domain of analytical and numerical investigations, early studies explored the application of the limit equilibrium method. Key contributions by Proctor and White (1977) and Ellstein (1986) focused on excavations under undrained conditions. Another noteworthy approach within the limit equilibrium framework, introduced by Anagnostou and Kovári (1994) and Anagnostou and Kovári (1996), utilized a frontal wedge model developed by Horn (1961). This model, in conjunction with the silo theory pioneered by Janssen (1895) and previously employed by Terzaghi (1943) under plane strain conditions, produced formulae for calculating the limit support pressure in cases where soils are acted upon under drained conditions.

Nowadays, the limit equilibrium method remains a valuable tool for studying the stability of the excavation front of shallow tunnels, as evidenced by recent works such as Zhang et al. (2020).

However, in addition to the imposition of sometimes unrealistic failure geometries, the limit equilibrium method often requires assumptions about the distribution of stresses in soils. While, in certain cases, the values obtained for the limit loads may align with the theoretical collapse load (as observed in the calculation of active earth pressures using the Coulomb wedge), it is generally not possible to determine beforehand whether the load estimated by a limit equilibrium method will be below or above the exact theoretical value of collapse.

Addressing this limitation, the results of the present work are grounded in the limit analysis method. To our knowledge, following

* Corresponding author.
E-mail address: amna@fct.unl.pt (A.N. Antão).

https://doi.org/10.1016/j.tust.2024.106137
Received 7 November 2023; Received in revised form 10 July 2024; Accepted 7 October 2024
Available online 23 October 2024

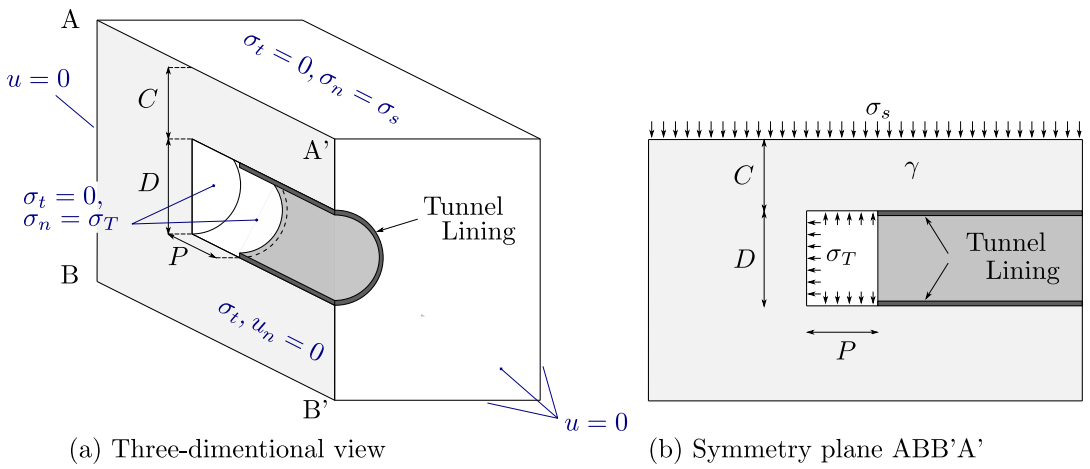

(a) Three-dimentional view (b) Symmetry plane ABB'A'

Fig. 1. Problem definition and static/kinematic boundary conditions.

the work of Atkinson and Potts (1977), who provided limit analysis solutions for the plane strain tunnel stability problem, Mühlhaus (1985), Leca and Panet (1988), and Leca and Dormieux (1990) can be regarded as pioneers in applying limit analysis to the heading stability of tunnels excavated in massifs with cohesive-frictional behavior. Since then, for about a decade, the only known work to us is that of Antão (1997), who established upper bounds for cases modeled in centrifuge by Chambon et al. (1991) and Chambon and Corté (1994). To the best of our knowledge, this is the first work published employing the Finite Elements Method applied to Limit Analysis for the study of 3D tunnel front stability.

At the beginning of the century, Subrin and Wong (2002) proposed a rotational type of collapse mechanism, introducing an improvement in the available upper-bound results at that time. However, it was not until the second decade of the present century that new works on limit analysis for the subject emerged as those of Mollon et al. (2010, 2011). These works primarily relied on the kinematic theorem, utilizing the Mohr–Coulomb (MC) criterion and numerical minimization of analytically defined mechanisms. More recently, Shiau and Al-Asadi (2020) proposed both lower and upper bounds for the stability load factors of tunnel excavation fronts under drained conditions, employing the Finite Elements Limit Analysis (FELA) method. As far as our information goes, the results presented by these authors are the most prominent for the addressed problem when treated with the MC criterion.

While widely used, the MC criterion possesses a notable limitation by failing to take properly into account the effect of the intermediate stress component. This particular constraint leads to an undervaluation of shear strength, especially when stress paths deviate from the classical triaxial compression path. To address this issue, various criteria have been proposed over time to better approximate experimental results. Among these, we find the Matsuoka-Nakai criterion (Matsuoka and Nakai, 1974, 1985), employed here in an extended form (Griffiths and Huang, 2009), henceforth referred to as the Extended-Matsuoka-Nakai (EMN) criterion, to address the possibility of the existence of effective cohesion, c'. This criterion has the advantage of coinciding with the Mohr–Coulomb criterion in the classic triaxial compression and the triaxial extension paths, thus allowing it to be possible to determine the shear strength properties through classic triaxial compression tests.

Very recently, Vicente da Silva and Antão (2023b) showed that, for the specific case of calculating the support pressure of the excavation face of a tunnel due to the unit weight of a soil mass with a friction angle of 30°, the difference between the results obtained using the MC and EMN criteria cannot be disregarded, indicating that the subject deserves further in-depth investigation.

Therefore, this study aims to present the results obtained for the stability of the excavation front under drained conditions of a circular tunnel. The analysis employs the EMN criterion for failure and resorts to the concept of stability factors. These factors were initially proposed for drained conditions by Atkinson and Potts (1981) and later extended by Anagnostou and Kovári (1996) to account for the existence of an effective cohesion.

2. Problem definition

In this paper, we address the stability of circular shallow tunnels. The geometry of the problem is defined in Fig. 1a. The tunnel has a diameter D, and its crown is at depth C. The distance between the rigid lining and the front is designated by P. Also indicated are the kinematic and static boundary conditions.

In Fig. 1b the charges acting on the soil are schematized: an uniform surface load σ_S, an uniform tunnel pressure σ_T acting on the unlined portion of the tunnel and the soil unit weight γ.

The tunnel is excavated under drained conditions in a soil considered fully saturated or completely dry. The soil's strength is modeled with the EMN criterion which represents a enhancement of the original proposal (Matsuoka and Nakai, 1974, 1985) where the criterion had a purely frictional character. In this work, a formulation that takes into account the existence of effective cohesion is used.

In the space of principal stresses, let equivalent principal stresses be defined by:

$$\overline{\sigma}_i = \sigma_i - \sigma_0\,, \quad i = \{I, II, III\} \tag{1}$$

where, σ_i is the principal stress component in the i direction, and σ_0 denotes the value of the maximum admissible hydrostatic pressure. The convention commonly adopted in geotechnics, indicating compression with positive values, is assumed throughout. With this definition, equivalent stress invariants are defined as:

$$\overline{I}_1 = \overline{\sigma}_I + \overline{\sigma}_{II} + \overline{\sigma}_{III} \tag{2}$$

$$\overline{I}_2 = \overline{\sigma}_I\overline{\sigma}_{II} + \overline{\sigma}_{II}\overline{\sigma}_{III} + \overline{\sigma}_{III}\overline{\sigma}_I \tag{3}$$

$$\overline{I}_3 = \overline{\sigma}_I\overline{\sigma}_{II}\overline{\sigma}_{III} \tag{4}$$

And the yield function is written as:

$$f(\overline{I}_1, \overline{I}_2, \overline{I}_3) = \overline{I}_1\overline{I}_2 - K_{MN}\overline{I}_3 \tag{5}$$

where, K_{MN} is a dimensionless material parameter. In order to the MC and EMN criteria to coincide in the case of classical triaxial loads, whether they are in compression or in extension, it is necessary that (Griffiths and Huang, 2009):

$$K_{MN} = \frac{9 - \sin^2(\phi')}{1 - \sin^2(\phi')} \tag{6}$$

$$\sigma_0 = -\frac{c'}{\tan(\phi')} \tag{7}$$

Following Shiau and Al-Asadi (2020), the minimum pressure to be exerted on the unsupported area of the tunnel to ensure its stability can be written as:

$$\sigma_T = \gamma D F_\gamma + \sigma_s F_s - c' F_{c'} \tag{8}$$

where F_γ, F_s and $F_{c'}$ are called stability factors.

This expression is the adaptation of one proposed by Atkinson and Potts (1981):

$$\sigma_T = \gamma D F_\gamma + \sigma_s F_s \tag{9}$$

for purely frictional materials and extended by Anagnostou and Kovári (1996) to take into account the existence of an effective cohesion, c'.

The determination of each one of the coefficients of the equation is done individually, in calculations that do not take into account the effects linked to other factors, that is:

- determination of $F_\gamma = \frac{\sigma_T}{\gamma D}$ in a calculation with $\sigma_s = 0$, $c' = 0$ and $\gamma \neq 0$
- determination of $F_S = \frac{\sigma_T}{\sigma_s}$ in a calculation with $\sigma_s \neq 0$, $c' = 0$ and $\gamma = 0$
- determination of $F_{c'} = -\frac{\sigma_T}{c'}$ in a calculation with $\sigma_s = 0$, $c' \neq 0$ and $\gamma = 0$

Eq. (8) is similar to the Terzaghi's bearing capacity of shallow foundations equation. It is based on the so-called superposition of effects. In the Terzaghi's bearing capacity equation, it is known that, in drained conditions, the use of that equation guarantees conservative results, on the safety side. The same is true for Eq. (8), or, to put it another way:

$$\begin{aligned}\sigma_T(\sigma_s \neq 0, c' \neq 0, \gamma \neq 0) \leq\ & \sigma_T(\sigma_s = 0, c' = 0, \gamma \neq 0) \\ & + \sigma_T(\sigma_s = 0, c' \neq 0, \gamma = 0) \\ & + \sigma_T(\sigma_s \neq 0, c' = 0, \gamma = 0)\end{aligned} \tag{10}$$

Attention must be given to the fact that Eq. (8) prevents a collapse in which the soil intrudes into the interior of the tunnel. If the value of σ_T applied to the unsupported part of the tunnel is too high, a blow-out type collapse may occur. However, it is important to note that this paper does not consider such situations.

3. Limit analysis numerical tool

The calculations presented in this paper employed a finite element implementation of the upper and lower-bound theorems of limit analysis. This choice was primarily driven by its capacity to rigorously establish the limit load of a mechanical structure. Although alternative methods such as incremental elasto-plastic analysis or limit equilibrium techniques can yield satisfactory solutions, accurately predicting whether these solutions fall below or exceed the precise limit load, and estimating their associated errors, remains a significant challenge.

The application of the limit analysis theorems relies on several classic assumptions. First, the material is assumed to be perfectly plastic, governed by a yield function denoted as $f(\sigma)$, which remains constant and unaffected by plastic strain, ϵ_p or strain rate $\dot{\epsilon_p}$. In addition, all plastic strain increments must always be normal to the yield surface, a principle known as the associated normal flow rule, which is expressed as follows: $\dot{\epsilon_p} = \lambda \frac{\partial f}{\partial \sigma}$, where λ is a positive parameter. Furthermore, the body is assumed to comply with the hypothesis of small perturbations.

The upper bound theorem allows us to define a load set where any load exceeding this range would invariably lead to structural collapse. In contrast, the lower bound theorem identifies a load range within which structural collapse is precluded. Combining these two theorems leads to the conclusion that the limit load falls within the range bounded by these two load sets. Thus, when these boundaries coincide, the precise collapse load becomes known — a corollary of the uniqueness theorem of limit analysis. This implies that precise results are achieved when the gap between the upper and lower regions is narrow, and its amplitude provides a direct error estimate for the obtained solutions.

Table 1
Three-field mixed finite element.

Element	velocity	strain rate	stress
UB	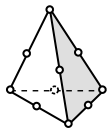	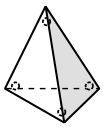	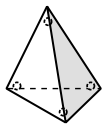
LB	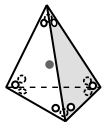	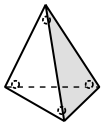	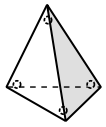

In this study, we employed a variant of the finite element limit analysis (FELA) formulation developed by the authors (Vicente da Silva et al., 2020). This upgraded version, with the capacity to accommodate the EMN criterion, was introduced in Vicente da Silva and Antão (2023b).

The development of FELA formulations entails translating the limit analysis theorems into a mathematical optimization problem, while simultaneously discretizing the continuum using finite elements. The lower-bound theorem requires that these elements have the capacity to generate statically admissible stress fields. Specifically, these stress fields must satisfy equilibrium conditions within the domain and across inter-element boundaries while meeting the yield criterion. On the other hand, the upper-bound elements should be capable of producing kinematically admissible velocity fields that conform to the normality condition.

The requirements described above impose significant constraints on the choice of finite elements suitable for designing rigorous FELA formulations. Our formulation relies on mixed tetrahedron elements for 3D analysis. These elements are termed 'mixed' because they independently approximate two related fields within the domain. To establish the connection between these two original fields, a third field of Lagrange multipliers is introduced into the model. By applying duality principles, it becomes possible to attribute physical significance to the Lagrange multipliers. The result is a three-field finite element, using nodal stresses, nodal plastic strains rate, and nodal velocities as variables. Piecewise linear polynomial functions are employed for the approximation of the strain rate and the stress field. For the velocity field, the upper-bound element employs quadratic polynomial approximation functions with C^0 continuity. In contrast, the lower-bound element employs a distinct and less conventional velocity approximation. The latter is constant within the element domain and varies linearly along each boundary, potentially resulting in discontinuous velocity fields. All the aforementioned approximations use nodal functions and variables and as a summary, the upper- and lower-bound elements are schematically represented in Table 1, with their nodal points.

The limit analysis problem, grounded in classical plasticity theory, gives rise to a mathematical convex optimization problem, and in the context of 2D and 3D continuum media, the yield condition consistently conveys a non-linear character to it.

The current numerical tool employs the Alternating Direction Method of Multipliers (ADMM) for the numerical solution of the Limit

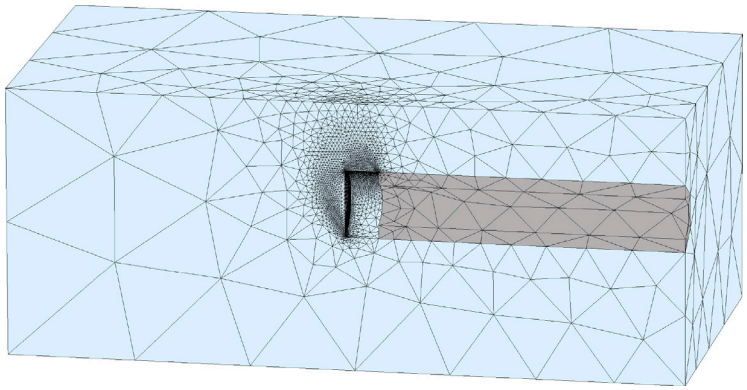

Fig. 2. Adaptive mesh example.

Analysis optimization problem. ADMM is an iterative algorithm known for its effectiveness in addressing complex optimization problems. It achieves this by decomposing the minimization task into two distinct steps, making use of the mixed finite element approximation.

The first step, referred to as Global minimization, entails the minimization of a quadratic functional determined by a system of linear equations that represent all mesh elements. Notably, the matrix associated with these equations remains unaltered throughout the iterative process, demanding only a single factorization.

The second step, named as Local minimization, deals with the nonlinear aspect of minimization, where the yield condition is enforced independently within each element of the mesh. This step can be tailored to optimize the method's efficiency, adapting to the specific requirements of the EMN criterion. ADMM's inherent characteristics render it a highly scalable algorithm suitable for parallel implementation. In this work, we leverage this scalability by employing parallel computing techniques to be able to address problems characterized by a substantial number of degrees of freedom, resulting in an ultimate improvement in the quality of computational results.

To further enhance the accuracy of the results, adaptive mesh refinement (AMR) is employed. This mesh refinement process, based on the methodology outlined in Martin (2011), aims to achieve uniform values of the integral of maximum absolute distortion for each element.

Fig. 2 displays the mesh obtained after five steps of the adaptive remeshing process for the determination of the upper-bound of F_γ, with parameters $P/D = 0.5$, $C/D = 1$, and $\phi' = 30°$. This mesh consists of approximately 62 thousand elements.

All mentioned features are integrated into our in-house software, mechpy (Vicente da Silva and Antão, 2023a). Fig. 3 outlines the computational procedure used to investigate the stability of tunnels with mechpy. In this scheme red arrows symbolize network communications.

4. Numerical results summary

The calculations were performed for the following geometrical parameters:

- $C/D \in \{0.5; 0.75; 1.0; 1.5; 2.0; 3.0\}$
- $P/D \in \{0; 0.1; 0.25; 0.5\}$

The values of C/D chosen are representative of shallow tunnels, although not covering the usual values for this geometrical configuration. But, except for the lower values of ϕ', the values of F_γ, F_S and $F_{c'}$ stabilize with the augmentation of C/D and therefore there is no need to perform the calculations for higher values of C/D.

In practice, the P/D value will hardly reach the highest values considered here. However, it was thought that it would be interesting to obtain these results to allow a better global understanding of the problem in question.

Concerning the mechanical strength of the soil mass, calculations were made for the following values of the shear strength angle:

$\phi' \in \{15°; 20°; 25°; 30°; 35; 40°; 45°\}$

The use of these values is intended to cover a wide range of values that can be found in drained load chargements.

Tables 2 to 4 present the results obtained for the three factors (F_γ, F_S and $F_{c'}$) for the different values of P/D studied. In general, the values given by the approximations of UB and LB are close to each other and delimit, from a practical point of view, the exact value of the stability factors quite well. Particularly in the case of $F_{c'}$, the approximations of LB and UB obtained, as they coincide one with another in many of the studied cases, allow defining the exact collapse load for those cases, except for inaccuracies of numerical origin.

More detailed comments about each of the stability factors are made in the following section.

5. Analysis and discussion of results

5.1. Factor F_γ

To initiate our analysis of the stability factor F_γ, Figs. 4 and 5 present the LB and UB approximations obtained for the stability factor F_γ versus C/D and ϕ', respectively, for all the values of P/D studied.

In general terms, it can be said that the value of F_γ increases with the increase of C/D for values of the friction angle lower than a given threshold. For values of ϕ' greater than this threshold, there is practically no influence of the relative depth on the F_γ value, which remains basically the same. This threshold increases slightly with the increase in the value of P/D, from $\phi' = 25°$ for $P/D = 0.0$ to $\phi' = 30°$ in the case of $P/D = 0.5$.

Even in cases where the F_γ value is influenced by C/D, this influence practically disappears for the studied P/D values, particularly at the highest C/D values. The exception to this pattern is observed in the case of $\phi' = 15°$. This trend is particularly noticeable in the largest P/D values, where F_γ does not stabilize with the increase of C/D.

Concerning the evolution of F_γ with ϕ', it consistently decreases with the increase of ϕ'. It shows low dependence on P/D, and for ϕ' greater than the mentioned threshold, it becomes independent of C/D.

These observations reveal a general behavior similar to that documented by other authors, irrespective of the method employed in their studies, using the MC criterion (Leca and Dormieux, 1990; Mollon et al., 2010, 2011; Shiau and Al-Asadi, 2020). In these studies, the spatial zone of the mechanism decreases with the increase of ϕ', a characteristic typically associated with active earth pressure loading conditions (Antão et al., 2016; Santana et al., 2023).

Concerning 3D tunnel stability, the global phenomenon appears to follow a similar pattern, albeit complicated by the geometric configuration of the tunnel. This complexity arises because the phenomenon may

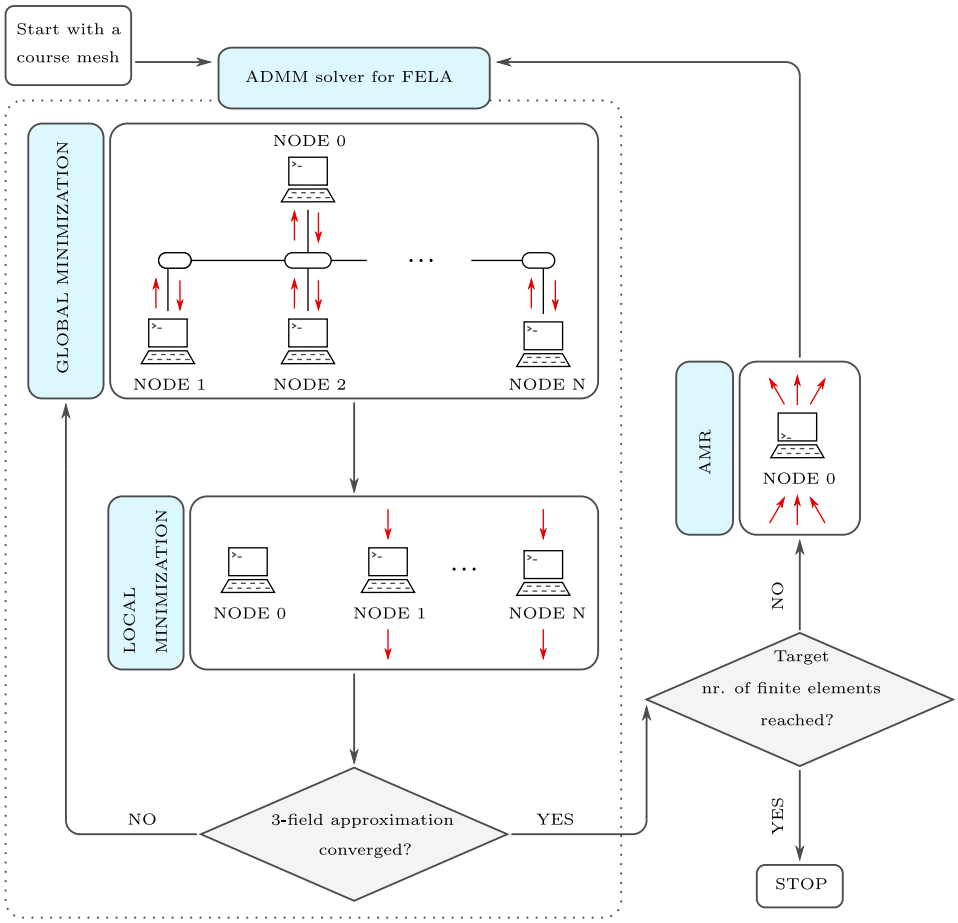

Fig. 3. Flowchart of the computational procedure.

Table 2
Lower and Upper bounds for F_γ.

P/D	ϕ'	$C/D = 0.5$		$C/D = 1.0$		$C/D = 1.5$		$C/D = 2.0$		$C/D = 3.0$	
		LB	UB	LB	UB	LB	UB	LB	UB	LB	UB
	15	0.344	0.327	0.373	0.351	0.389	0.370	0.398	0.370	0.411	0.379
	20	0.237	0.222	0.244	0.227	0.247	0.229	0.247	0.229	0.249	0.229
	25	0.167	0.155	0.168	0.155	0.168	0.155	0.168	0.155	0.168	0.155
0	30	0.121	0.111	0.121	0.111	0.121	0.111	0.121	0.111	0.121	0.110
	35	0.088	0.080	0.088	0.080	0.088	0.080	0.088	0.080	0.088	0.080
	40	0.065	0.058	0.065	0.058	0.065	0.058	0.065	0.058	0.065	0.058
	45	0.047	0.041	0.047	0.041	0.047	0.041	0.047	0.041	0.047	0.041
	15	0.350	0.333	0.391	0.365	0.408	0.381	0.421	0.391	0.436	0.404
	20	0.243	0.228	0.255	0.236	0.258	0.238	0.259	0.238	0.258	0.239
	25	0.172	0.157	0.173	0.160	0.174	0.160	0.174	0.158	0.174	0.160
0.1	30	0.123	0.113	0.123	0.112	0.123	0.112	0.124	0.113	0.123	0.114
	35	0.090	0.081	0.090	0.080	0.090	0.081	0.090	0.081	0.090	0.081
	40	0.066	0.058	0.066	0.058	0.066	0.057	0.066	0.058	0.066	0.058
	45	0.048	0.041	0.048	0.041	0.048	0.041	0.048	0.041	0.048	0.040
	15	0.356	0.339	0.405	0.384	0.438	0.402	0.455	0.422	0.478	0.439
	20	0.251	0.237	0.269	0.248	0.273	0.249	0.279	0.254	0.281	0.256
	25	0.178	0.165	0.184	0.166	0.184	0.167	0.184	0.167	0.184	0.167
0.25	30	0.128	0.115	0.129	0.116	0.129	0.116	0.129	0.116	0.129	0.113
	35	0.093	0.082	0.094	0.082	0.093	0.082	0.093	0.082	0.093	0.082
	40	0.068	0.059	0.068	0.059	0.068	0.058	0.067	0.059	0.068	0.058
	45	0.050	0.041	0.050	0.041	0.049	0.041	0.050	0.042	0.049	0.041
	15	0.370	0.346	0.454	0.416	0.495	0.454	0.529	0.477	0.554	0.508
	20	0.270	0.247	0.306	0.275	0.321	0.286	0.328	0.290	0.328	0.296
	25	0.199	0.176	0.213	0.186	0.215	0.187	0.216	0.188	0.214	0.190
0.5	30	0.148	0.126	0.152	0.129	0.152	0.129	0.152	0.129	0.149	0.130
	35	0.113	0.094	0.115	0.094	0.113	0.094	0.113	0.094	0.109	0.095
	40	0.089	0.072	0.088	0.072	0.088	0.072	0.088	0.072	0.085	0.072
	45	0.069	0.054	0.070	0.055	0.070	0.054	0.070	0.054	0.067	0.055

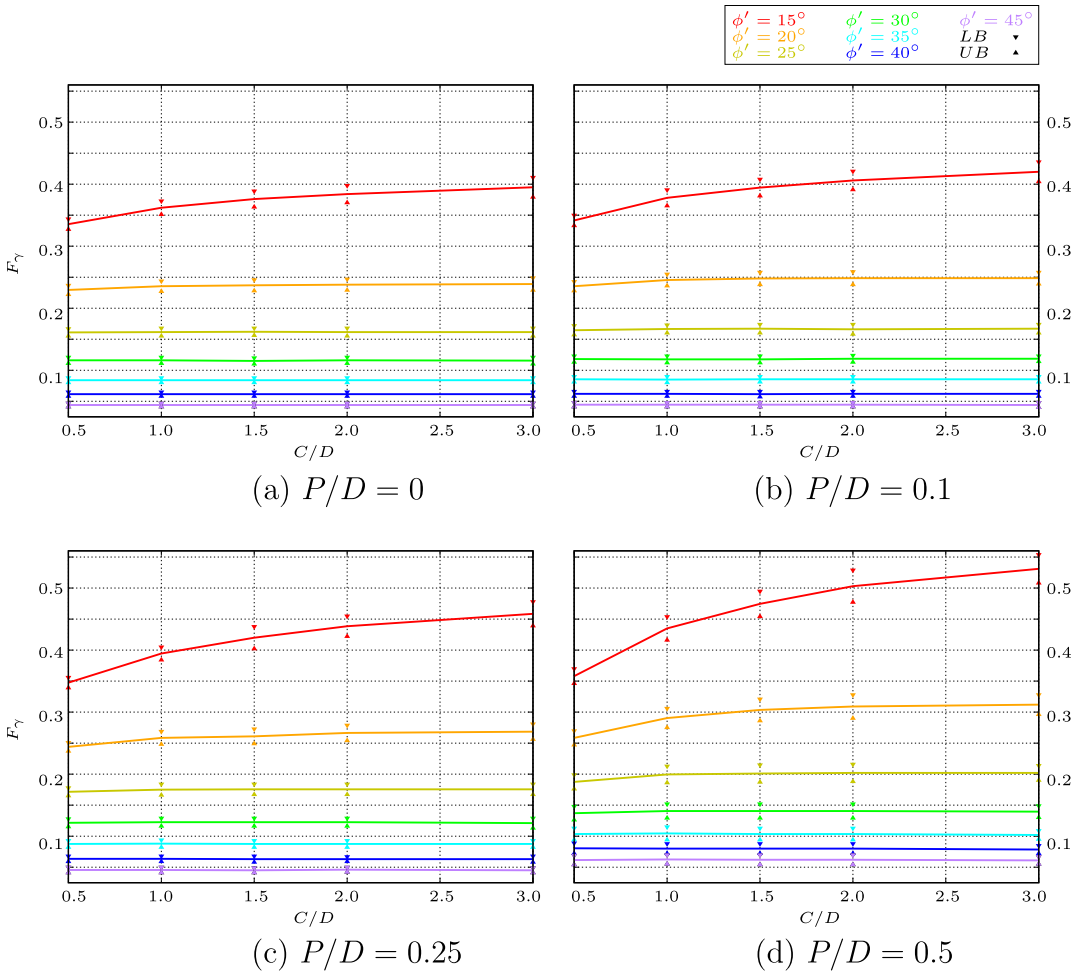

Fig. 4. Evolution of F_γ as a function of C/D for different values of P/D. (For interpretation of the references to color in this figure legend, the reader is referred to the web version of this article.)

or may not be influenced by the boundaries of the massif. Additionally, the relief of stresses is likely to occur predominantly in the horizontal or sub-horizontal directions.

In the following figures, we illustrate these ideas with representations of the collapse mechanisms obtained.

Figs. 6 to 9 depict the value of the maximum plastic distortion rate, $\max(\dot{\varepsilon}_p^I - \dot{\varepsilon}_p^{III})$, a measure of soil deformation, for various geometrical cases and two different values of ϕ'. These figures, along with those in the subsequent sections, provide insight into the spatial development of collapse mechanisms.

For all cases depicted, the zone involving the mechanism for $\phi' = 20°$ is larger than the one for $\phi' = 40°$.

When these mechanisms do not reach the top surface, their characteristics do not change with the increase of C/D. In the case of this stability factor, the external forces acting include the unit weight and the support pressure on the unsupported surface. If the development of the mechanism remains unchanged with the increase in C/D, it is expected that the balance between the different loads remains constant, resulting in a consistent outcome in the calculations.

This suggests that the aforementioned threshold is directly related to the geometrical configuration, particularly to its cover depth, C, at which the mechanism stops reaching the surface.

The geometrical configuration at which the mechanism stops reaching the surface is linked not only to the value of the friction angle but also to the value of P/D. An increase in this parameter induces a change in the mechanism: it transitions from developing exclusively on the excavation front part to a mechanism in which, alongside the excavation front, there is a contribution from the tunnel body without lining. In certain cases, there is even a preponderance of the mechanism in the unlined part of the tunnel, overshadowing the development at the excavation front.

The existence of these mixed mechanisms (collapse in the excavation front and in the unsupported body of the tunnel) appears to facilitate their extension to the surface, thereby increasing the value of the ϕ' threshold mentioned above.

Finally, it is observed that the approximation between the values provided by the UB and LB calculations is greater for higher friction angles. This is likely due to the mechanisms having smaller spatial dimensions in materials with higher friction angles. Consequently, for a similar number of finite elements used, more refined meshes can be applied in the mechanism area in these cases.

5.2. Factor F_S

The plots in Figs. 10 and 11 depict the LB and UB approximations for the stability factor F_S with respect to C/D and ϕ', respectively, for the investigated values of P/D. It is important to observe that the values of F_S are displayed on a logarithmic scale in these figures.

It is evident that the order of magnitude of F_S can be quite small. Similar to the behavior of the F_γ factor, F_S decreases with an increasing friction angle. However, in contrast to F_γ, F_S decreases as C/D increases.

It is worth noting that F_S represents the ratio between the necessary support force applied in the excavation zone and the load applied to the

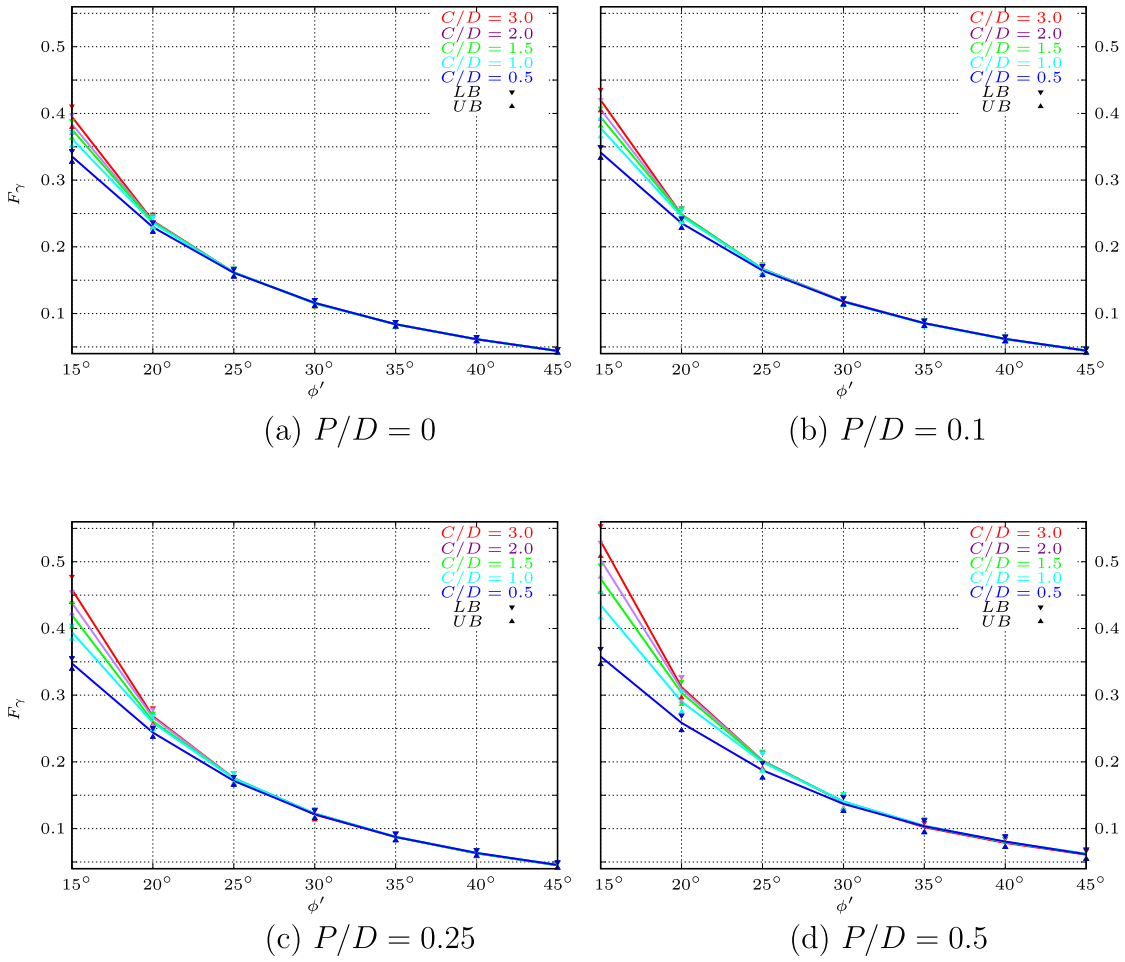

Fig. 5. Evolution of F_γ as a function of ϕ' for different values of P/D. (For interpretation of the references to color in this figure legend, the reader is referred to the web version of this article.)

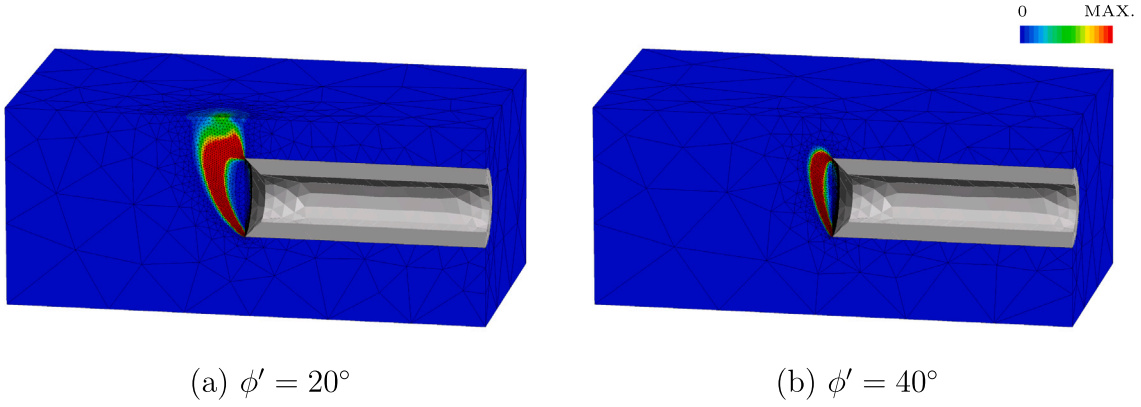

Fig. 6. Plastic deformation on the calculation of F_γ for $P/D = 0$ and $C/D = 0.5$.

surface. Now, the greater the distance from the tunnel to the surface, the smaller the influence of this load and, consequently, the smaller the F_S.

In the presented results, the lower value of F_S was constrained to 10^{-3} for two primary reasons: firstly, values below this threshold are deemed to have a negligible effect on the front support pressure; secondly, obtaining accurate values for this stability factor in such cases proved to be challenging from a numerical standpoint.

Once again, this behavior is linked to the failure mechanism which, by not propagating to the surface, prevents the surface loads to play a role in the collapse of the tunnel. In reality, this phenomenon is direct evidence of the so-called arch effect.

Figs. 12 and 13 show the mechanisms for the same values of the friction angle and P/D as before. The general trends are similar to those observed in the case of $F\gamma$: the mechanisms decrease with increasing friction angle and increase with increasing P/D. In fact, for the $\phi' = 40°$ case in these figures, since the mechanism does not reach the

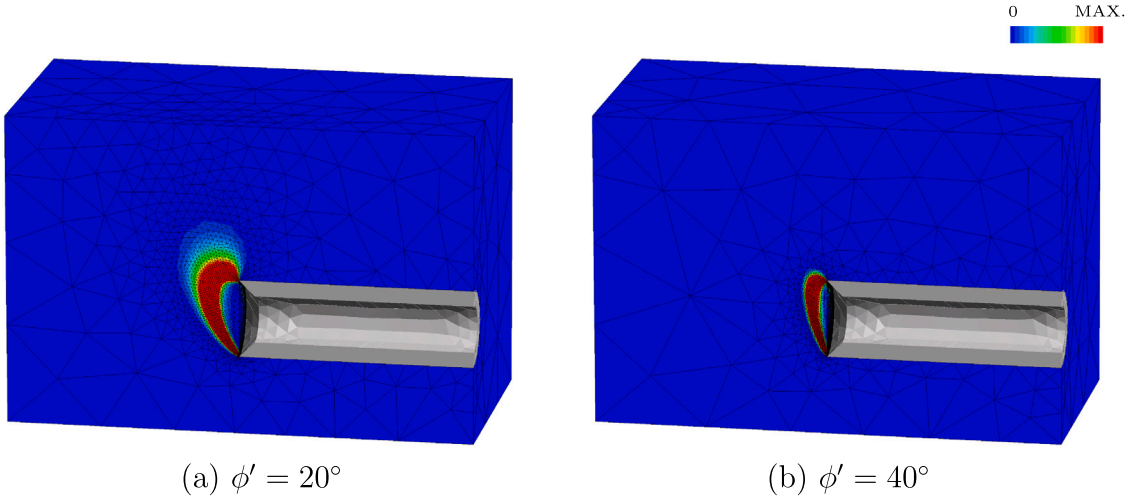

Fig. 7. Plastic deformation on the calculation of F_γ for $P/D = 0$ and $C/D = 2.0$.

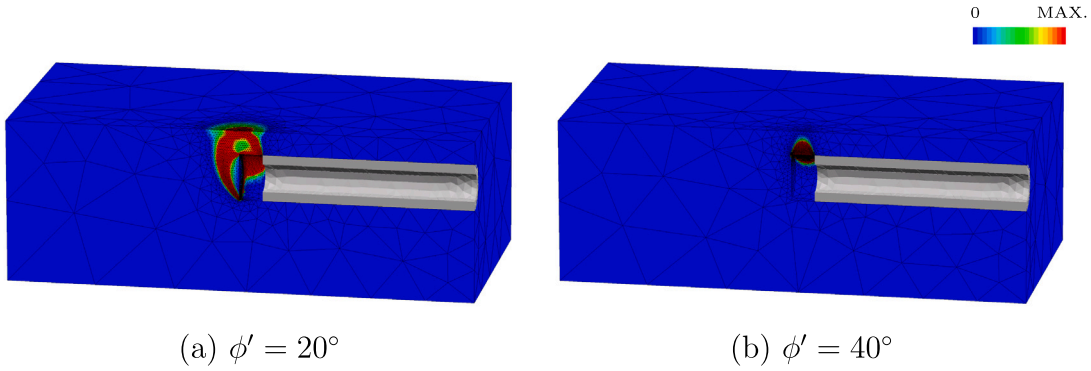

Fig. 8. Plastic deformation on the calculation of F_γ for $P/D = 0.5$ and $C/D = 0.5$.

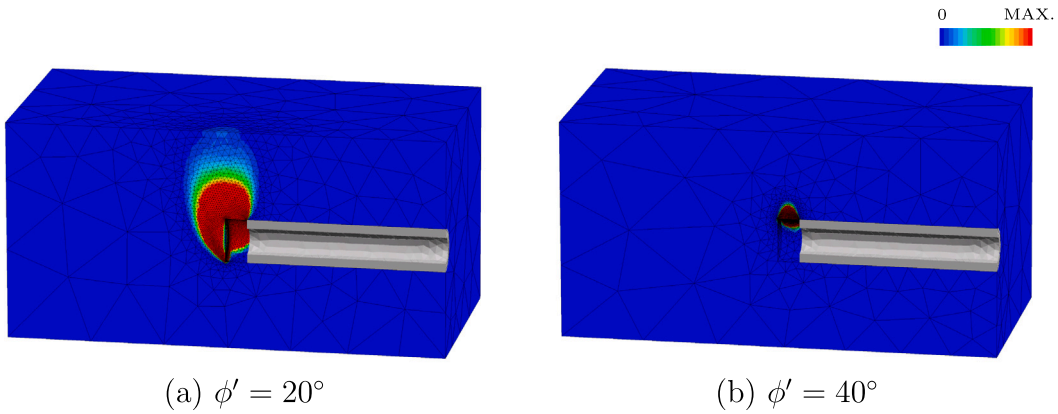

Fig. 9. Plastic deformation on the calculation of F_γ for $P/D = 0.5$ and $C/D = 2.0$.

surface, surface loading should not generate any power, implying that the applied pressure in the tunnel should be zero. However, in reality, there is some deformation at the surface, but it is so small that it is not discernible on the color scale used.

5.3. Factor $F_{c'}$

Figs. 14 and 15 show the evolution of $F_{c'}$ as a function of C/D and ϕ', respectively, for the different P/D cases studied. Unlike previous presentations, all P/D values are shown in the same figure, as the influence of P/D on the results is minimal for lower ϕ' values (smaller than 30°) and virtually non-existent for all the other friction angles. Further departing from earlier plots and with the goal of improving the readability of Fig. 15, we have excluded the upper and lower bound points, presenting only the average curves in this particular case.

As in the case of F_γ, the value of $F_{c'}$ increases with increasing C/D and decreases with increasing friction angle. However, remember that, given the negative sign of the c' term in Eq. (8), the influence of this term translates into a smaller support pressure necessary to apply to sustain the tunnel.

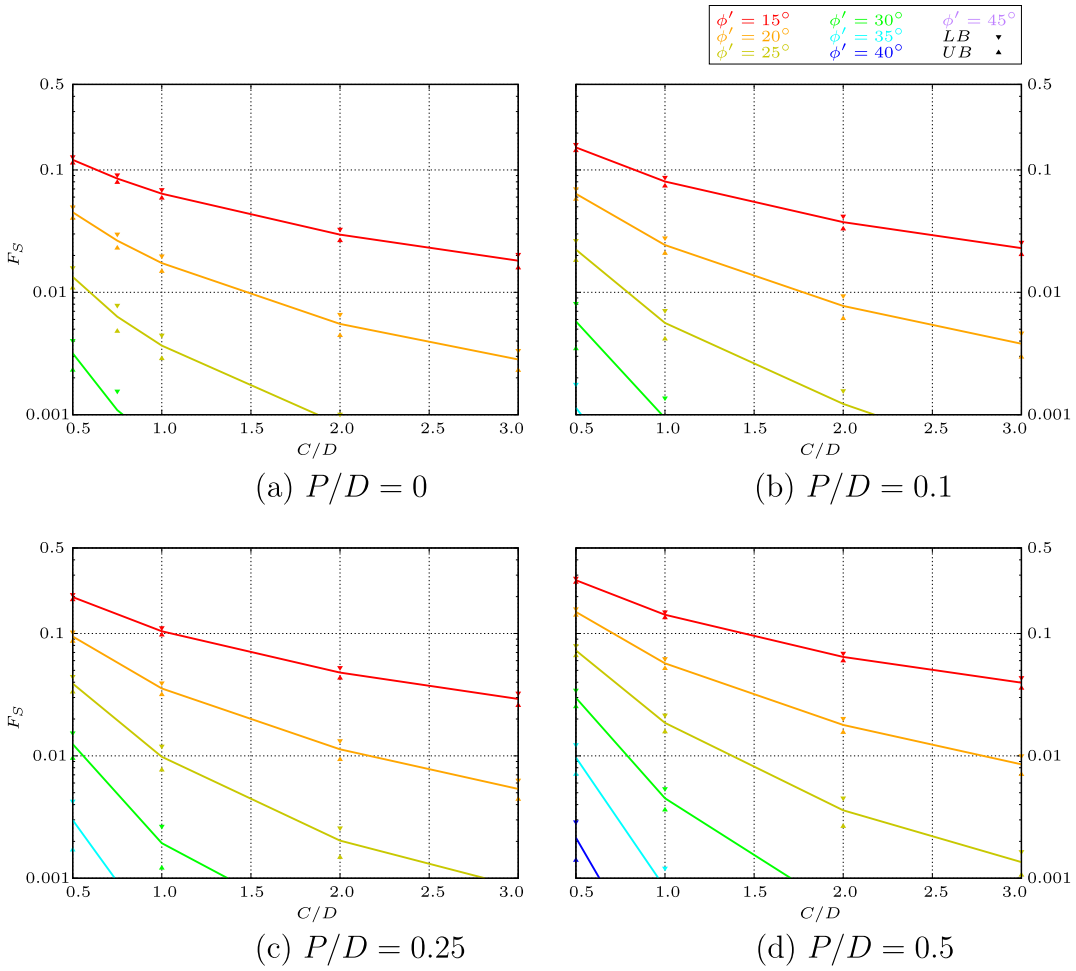

Fig. 10. Evolution of F_S as a function of C/D for different values of P/D. (For interpretation of the references to color in this figure legend, the reader is referred to the web version of this article.)

It is worth noting that, for each value of friction angle, for values of C/D greater than a given threshold, the value of $F_{c'}$ tends to be equal to $\cot(\phi')$. This means that, regardless of the value of P/D, if the mechanism is contained in the soil mass the value of the factor $F_{c'}$ is known. It should be mentioned that the values of Shiau and Al-Asadi (2020), although based on the MC criterion, seem to point to the same result. This coincidence should only be possible if all the stress states involved were triaxial compression or extension, the only cases in which the MC and MN criteria coincide. A closer analysis made it possible to show that in reality the tensions involved were associated with the point of intersection of the coincident states in the two aforementioned criteria, which is their apex, where the orientation of the strains offers multiple possibilities. This finding raises, however, the question of the usefulness and applicability of the $F_{c'}$, given that in a calculation involving the unit weight of the soil and, eventually, the σ_S, the mechanism would hardly have a similar configuration.

5.4. Comparison with other authors' results

In the next two sections of the paper, the comparison of our results is made both with results obtained experimentally and with Limit Analysis results from calculations made on the same stability problem, despite being carried out with another yield criterion.

5.4.1. Comparison with experimental results

This section presents a comparative analysis between the outcomes of our study and experimental results available in the literature, conducted on scaled-down models. The models were either subjected to the acceleration of gravity or the acceleration produced by a centrifuge. The comparison involves certain complexities, particularly in estimating the soil's shear strength parameters during the tests. In some studies, such details are not provided; the materials are solely classified as dense or loose. Our focus, therefore, was on studies providing estimates of the friction angle, a primary shear strength parameter for soils like sand. While these soils may exhibit a non-zero apparent cohesion value, often linked to moisture presence, we opted not to consider it in our presented results. But even in works where a friction angle is provided, it is difficult to understand what its nature is, especially with regard to saying whether it is a critical state friction angle or a peak state friction angle.

The experimental works chosen were those of Chambon and Corté (1994), Kirsch (2010) and Chen et al. (2013) for the case $P/D = 0$ and Chambon et al. (1991) for the case $P/D > 0$.

Chambon and Corté (1994) conducted multiple centrifuge tests, varying the compactness of sand and simulating different diameters and relative depths. While not explicitly stated, it can be inferred that the reported friction angles correspond to peak angles, as they refer to the challenges encountered in evaluating the angles under test conditions. According to their findings, the friction angles ranged from 38 to 42°. But they also took into account the potential presence of a slight moisture content in the materials, which could result in an apparent cohesion of up to 5 kPa. The results of these authors are compared with those of the present work in Fig. 16. It should be noted that the authors present in this set of values some obtained with P/D slightly higher than zero, which they say are indistinguishable from the results

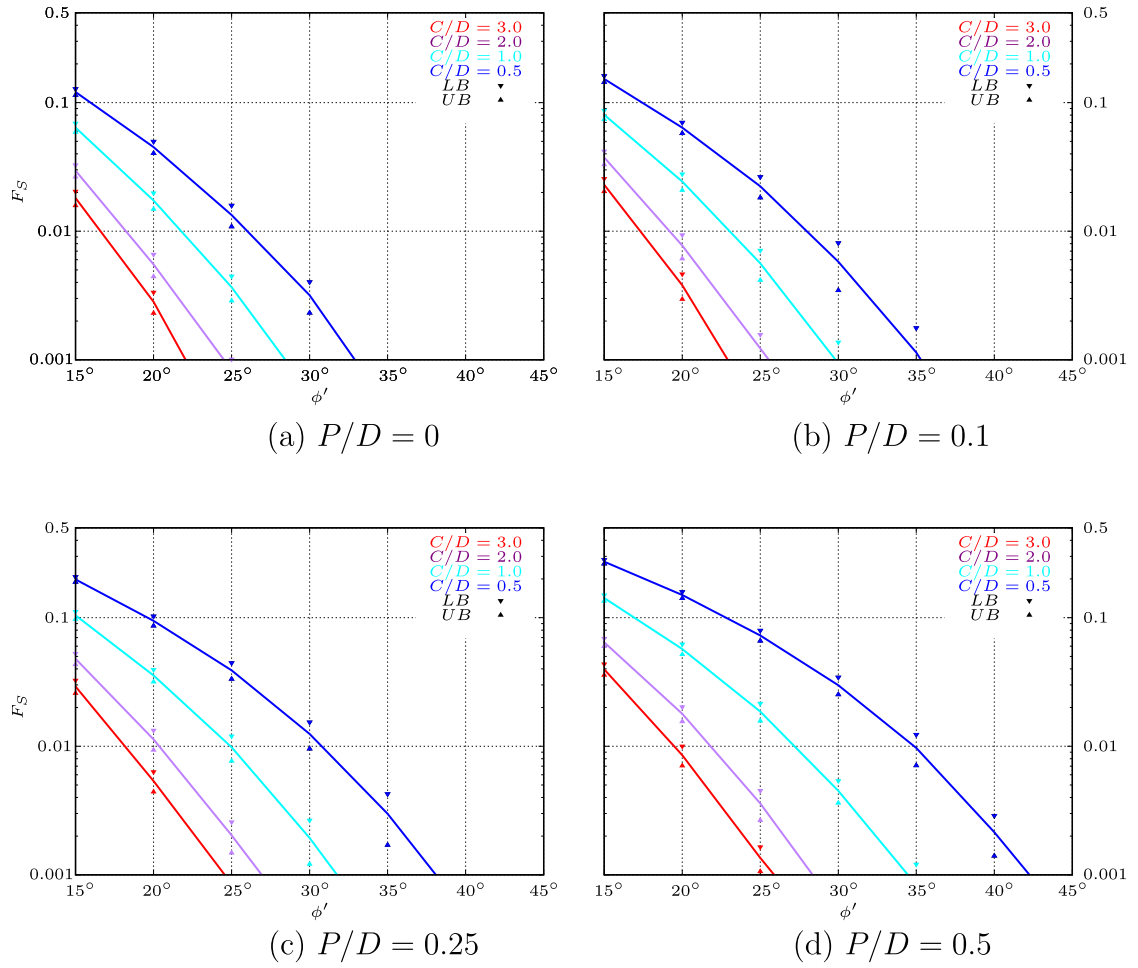

Fig. 11. Evolution of F_S as a function of ϕ' for different values of P/D. (For interpretation of the references to color in this figure legend, the reader is referred to the web version of this article.)

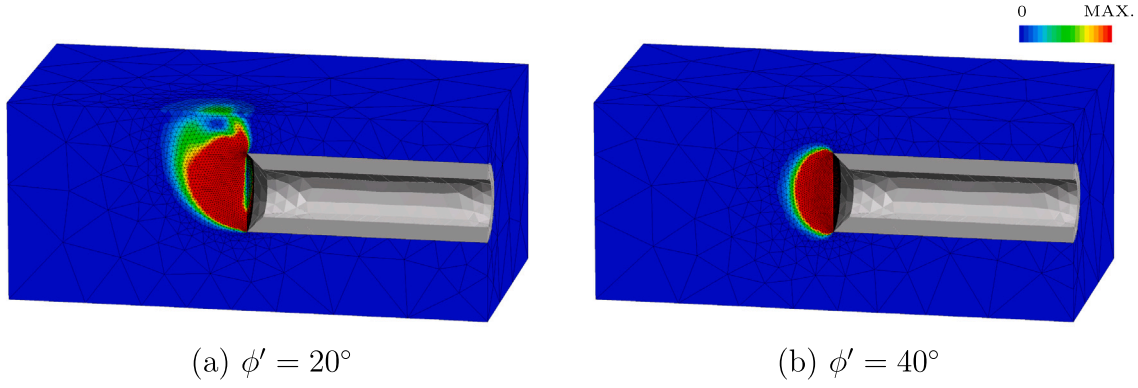

Fig. 12. Plastic deformation on the calculation of F_S for $P/D = 0.0$ and $C/D = 0.5$.

obtained for $P/D = 0$. They also present some results for $C/D = 4$ and that we decided to keep because, as seen previously, for the ϕ' values in question our results remain constant with the variation of C/D. In all cases, even in comparison with other authors, the results presented correspond to the quotient between the limit pressure applied in the tunnel and the product of the unit weight by the diameter of the tunnel. This value corresponds to the value of F_γ if the load applied to the surface as well as the effective cohesion are null. In case an effective cohesion is considered, the comparison is not direct, but our values would suffer a decrease in relation to our values of F_γ.

The comparison with our results shows that the experimental results of Chambon and Corté (1994) are reasonably delimited by our results for $\phi' = 40°$ and $\phi' = 45°$. Considering the implications highlighted in the previous section regarding the influence of cohesion on our results, it appears that the comparison between the experimental findings and ours is quite satisfactory.

Kirsch (2010) presents results from 52 tests on a reduced model, considering two different materials. The critical friction angles reported are $\phi' = 31.3°$ and $\phi' = 32.5°$. In the experimental tests on loose and dense sands, it is evident from the results that the tunnel pressure tends to converge to the same value with the increase of the tunnel's front

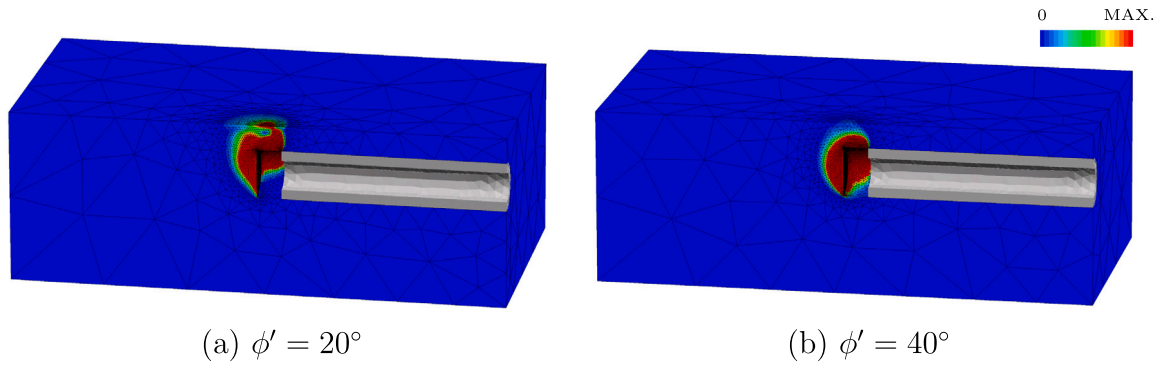

Fig. 13. Plastic deformation on the calculation of F_S for $P/D = 0.5$ and $C/D = 0.5$.

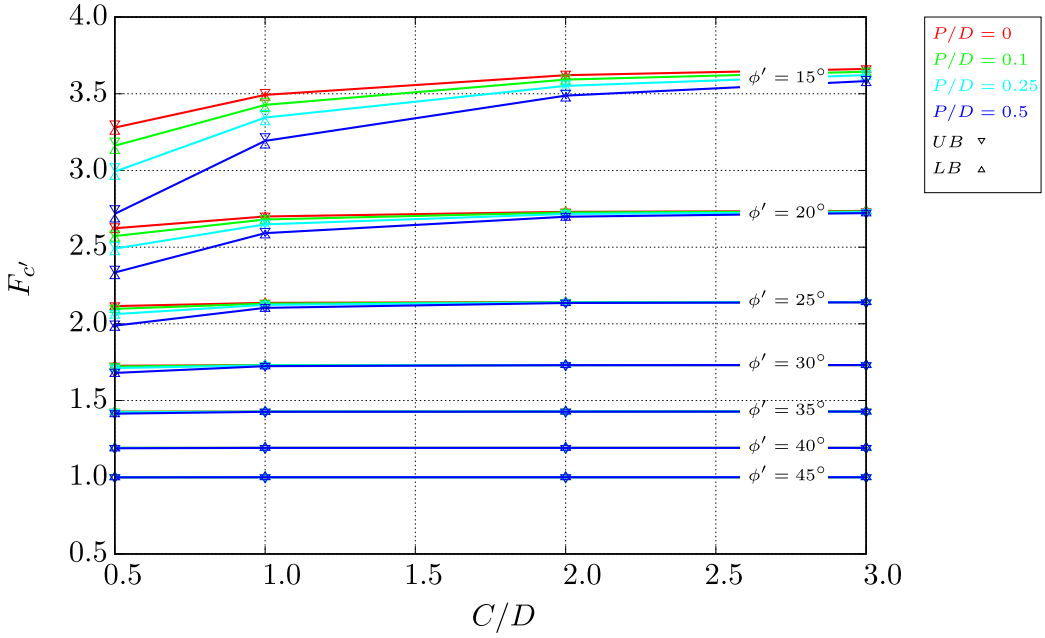

Fig. 14. Evolution of $F_{c'}$ as a function of C/D. (For interpretation of the references to color in this figure legend, the reader is referred to the web version of this article.)

deformation, likely when the mobilized friction angle matches the critical value friction angle. However, in the initial stages of deformation, there is a notable difference in the support pressure required for loose and dense materials. This leads us to believe that, for a more accurate prediction in these initial moments of collapse, having the values of the peak friction angles would be necessary. In their presentation, Kirsch (2010) displays the results as vertical bars for each experiment. In our graph, we opted to represent all experimental data with multiple values for the same friction angle using a single data point, obtained by averaging the extremum values. A vertical bar accompanies this point, visually indicating the amplitude of the experimental dispersion.

As illustrated in Fig. 16, the dispersion in the results of Kirsch (2010) is considerable. This implies that some values from their work align with the presented results, while others distinctly deviate from the predictions made in their study.

Chen et al. (2013) also present three test results in reduced model. From what was described in the work of these authors, it appears that the friction angle shown, $\phi' = 37°$, is a peak value. As for the effective cohesion of the material, it is considered null, although the author, in some of their calculations, considers a slight value for this parameter (0.5 kPa) considering that they refer to the fact that the sand used was not completely dry. The observation of Fig. 16 allows to verify that Chen et al. (2013) experimental results are perfectly framed by the calculations with $\phi' = 35°$ and $\phi' = 40°$.

Considering results corresponding to values of P/D greater than 0, we examined those presented by Chambon et al. (1991). The geometric parameter C/D is equal to 4 and P/D is equal to 0.1, 0.2 and 0.4. The tests were carried out on standard sand from the University of Bochum, which has a $\phi' = 36.5°$ value and a unit weight of 16.7 kN/m^3 (König et al., 1991).

The results are shown in Fig. 17. It can be seen that our results obtained with $\phi' = 40°$ fit well with the experimental results for $P/D = 0.1$ and $P/D = 0.2$. However, in the case of $P/D = 0.4$ the experimental results clearly deviate from the results obtained in this work, showing a limit pressure in the tunnel that is higher than the value obtained for $\phi' = 35°$ and even greater than the results for $\phi' = 30°$.

5.4.2. Comparison with limit analysis results

The bibliographical research carried out on the stability of tunnels in drained conditions did not allow us to uncover any Limit Analysis work on the subject using the EMN criterion. In reality, it was not possible to find analytical or numerical work on the subject, which prevents a direct comparison with other similar results.

However, to situate our results in relation to those available in the literature Fig. 16, in addition to the experimental results mentioned

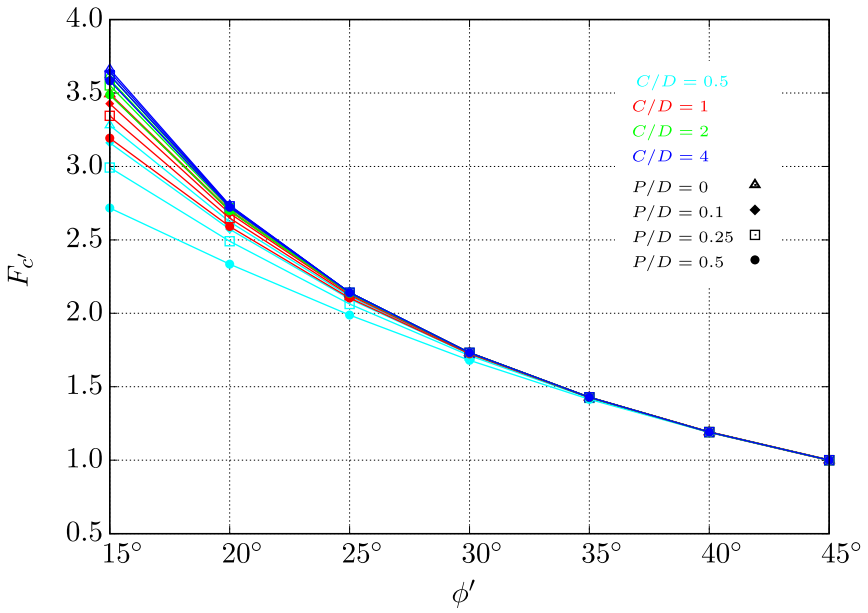

Fig. 15. Evolution of $F_{c'}$ as a function of ϕ'. (For interpretation of the references to color in this figure legend, the reader is referred to the web version of this article.)

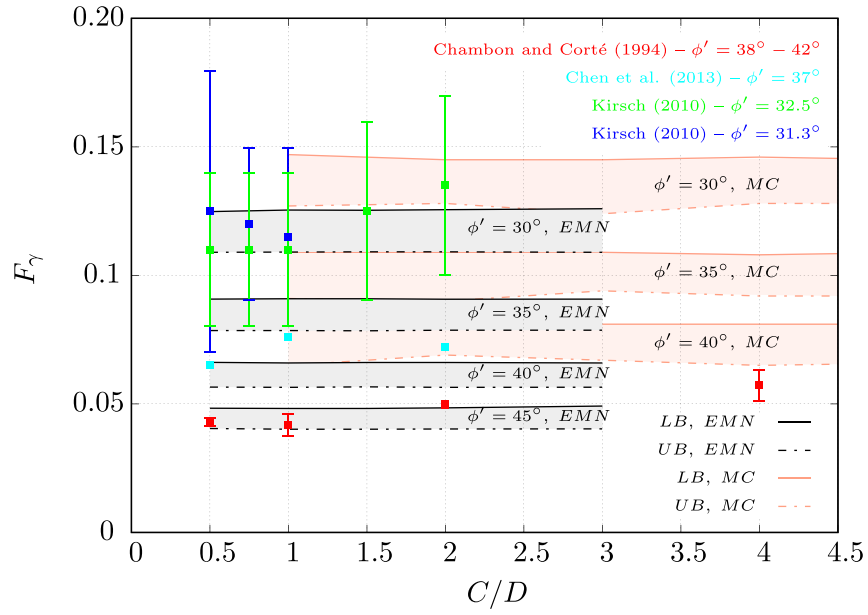

Fig. 16. Comparison of F_γ with experimental results for $P/D = 0$. (For interpretation of the references to color in this figure legend, the reader is referred to the web version of this article.)

above, illustrates the computational results obtained by Shiau and Al-Asadi (2020) using commercial FELA software and applying the MC criterion. It is noteworthy that these authors do not provide results for C/D smaller than 1. As evident, the MC criterion tends to underestimate tunnel strength stability compared to EMN results, with EMN demonstrating a closer alignment with the experimental data.

6. Concluding remarks

The present work aimed to study the stability of tunnels excavated in soil, in drained conditions. The research was conducted within the framework of limit analysis, a method that provides rigorous upper- and lower-bounds for the limit load of mechanical structures.

To assess stability, we employed stability factors, each representing the impact of specific factors such as the soil's unit weight, the presence of surface loads, and the potential existence of effective cohesion intercepts. Notably, our study introduced a significant innovation by utilizing the Extended Matsuoka-Nakai (EMN) criterion to characterize the shear strength properties of the material in drained conditions. To the best of our knowledge, prior research exclusively relied on the Mohr–Coulomb criterion, which has known limitations in representing the influence of intermediate stress on material shear strength.

Using the FELA program in conjunction with the EMN criterion, we explored the effects of varying geometric and shear strength parameters. This analysis generated a set of factors that hold practical value for engineering applications.

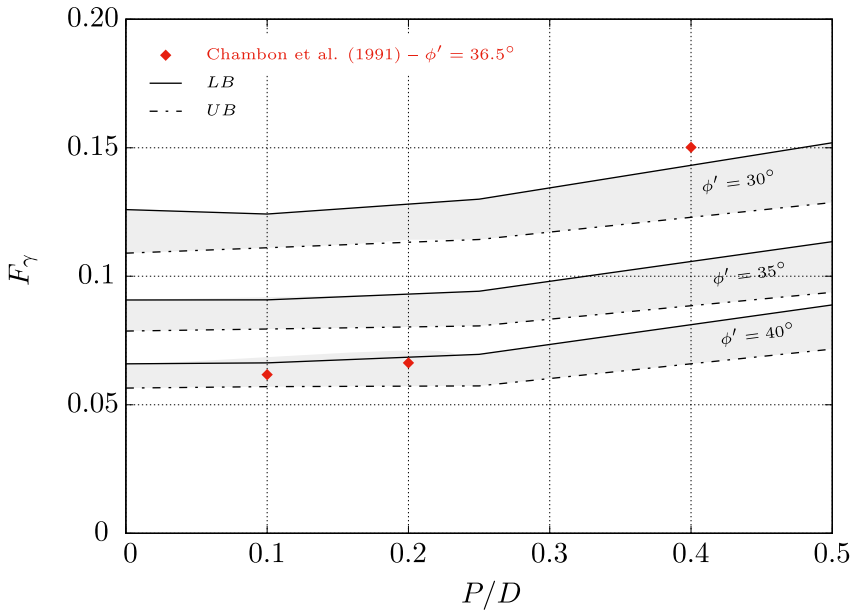

Fig. 17. Comparison of F_γ with experimental results for $P/D \neq 0$.

Table 3
Lower and Upper bounds for F_S.

P/D	ϕ'	$C/D = 0.5$		$C/D = 1.0$		$C/D = 2.0$		$C/D = 3.0$	
		LB	UB	LB	UB	LB	UB	LB	UB
	15	0.128	0.114	0.069	0.059	0.033	0.026	0.020	0.016
	20	0.050	0.040	0.020	0.015	0.007	0.004	0.003	0.002
	25	0.016	0.011	0.004	0.003	0.001	0.001	0.000	0.000
0	30	0.004	0.002	0.001	0.000	0.000	0.000	0.000	0.000
	35	0.001	0.000	0.000	0.000	0.000	0.000	0.000	0.000
	40	0.000	0.000	0.000	0.000	0.000	0.000	0.000	0.000
	45	0.000	0.000	0.000	0.000	0.000	0.000	0.000	0.000
	15	0.162	0.144	0.087	0.074	0.042	0.033	0.026	0.020
	20	0.070	0.058	0.028	0.021	0.009	0.006	0.005	0.003
	25	0.027	0.018	0.007	0.004	0.002	0.001	0.001	0.000
0.1	30	0.008	0.003	0.001	0.001	0.000	0.000	0.000	0.000
	35	0.002	0.001	0.000	0.000	0.000	0.000	0.000	0.000
	40	0.000	0.000	0.000	0.000	0.000	0.000	0.000	0.000
	45	0.000	0.000	0.000	0.000	0.000	0.000	0.000	0.000
	15	0.208	0.189	0.112	0.097	0.053	0.043	0.033	0.026
	20	0.103	0.086	0.039	0.032	0.013	0.009	0.006	0.004
	25	0.045	0.033	0.012	0.008	0.003	0.001	0.001	0.001
0.25	30	0.015	0.010	0.003	0.001	0.000	0.000	0.000	0.000
	35	0.004	0.002	0.000	0.000	0.000	0.000	0.000	0.000
	40	0.001	0.000	0.000	0.000	0.000	0.000	0.000	0.000
	45	0.000	0.000	0.000	0.000	0.000	0.000	0.000	0.000
	15	0.283	0.262	0.150	0.135	0.069	0.060	0.044	0.036
	20	0.159	0.141	0.062	0.052	0.020	0.016	0.010	0.007
	25	0.080	0.066	0.022	0.016	0.005	0.003	0.002	0.001
0.5	30	0.034	0.025	0.005	0.004	0.001	0.000	0.000	0.000
	35	0.012	0.007	0.001	0.000	0.000	0.000	0.000	0.000
	40	0.003	0.001	0.000	0.000	0.000	0.000	0.000	0.000
	45	0.001	0.000	0.000	0.000	0.000	0.000	0.000	0.000

Table 4
Lower and Upper bounds for $F_{c'}$.

P/D	ϕ'	$C/D = 0.5$		$C/D = 1.0$		$C/D = 2.0$		$C/D = 3.0$	
		LB	UB	LB	UB	LB	UB	LB	UB
	15	3.252	3.307	3.473	3.512	3.610	3.631	3.656	3.667
	20	2.610	2.637	2.693	2.706	2.729	2.732	2.738	2.734
	25	2.110	2.121	2.135	2.139	2.142	2.141	2.142	2.141
0	30	1.725	1.729	1.731	1.731	1.731	1.731	1.731	1.731
	35	1.427	1.428	1.428	1.428	1.428	1.428	1.428	1.428
	40	1.192	1.192	1.192	1.192	1.191	1.192	1.191	1.192
	45	1.000	1.000	1.000	1.000	1.000	1.000	1.000	1.000
	15	3.127	3.195	3.400	3.455	3.577	3.606	3.636	3.651
	20	2.555	2.590	2.671	2.690	2.723	2.729	2.734	2.730
	25	2.089	2.105	2.129	2.135	2.141	2.141	2.143	2.141
0.1	30	1.719	1.725	1.730	1.731	1.732	1.731	1.732	1.731
	35	1.426	1.427	1.428	1.428	1.428	1.428	1.428	1.428
	40	1.191	1.192	1.192	1.192	1.192	1.192	1.192	1.192
	45	1.000	1.000	1.000	1.000	1.000	1.000	1.000	1.000
	15	2.957	3.028	3.314	3.375	3.535	3.569	3.610	3.633
	20	2.466	2.514	2.637	2.660	2.711	2.721	2.729	2.728
	25	2.053	2.073	2.119	2.128	2.139	2.140	2.142	2.140
0.25	30	1.708	1.715	1.727	1.730	1.731	1.731	1.732	1.731
	35	1.422	1.426	1.427	1.428	1.428	1.428	1.428	1.428
	40	1.191	1.192	1.192	1.192	1.192	1.192	1.192	1.192
	45	1.000	1.000	1.000	1.000	1.000	1.000	1.000	1.000
	15	2.679	2.754	3.162	3.224	3.468	3.507	3.569	3.597
	20	2.310	2.360	2.576	2.606	2.691	2.705	2.719	2.725
	25	1.973	2.003	2.097	2.111	2.134	2.138	2.141	2.139
0.5	30	1.672	1.688	1.722	1.726	1.731	1.731	1.732	1.731
	35	1.411	1.418	1.426	1.428	1.428	1.428	1.428	1.428
	40	1.187	1.190	1.192	1.192	1.192	1.192	1.192	1.192
	45	0.999	1.000	1.000	1.000	1.000	1.000	1.000	1.000

In conclusion, our comparison with experimental results suggests that our proposed methodology shows promising applicability in the examined cases. Additionally, the comparison with experimental data indicates that our approach offers advantages over the conventional MN approach, representing a valuable contribution to this field.

CRediT authorship contribution statement

A.N. Antão: Conceptualization, Formal analysis, Investigation, Writing – original draft, Writing – review & editing. **M. Vicente da Silva:** Formal analysis, Investigation, Writing – original draft, Writing – review & editing.

Declaration of competing interest

The authors declare that they have no known competing financial interests or personal relationships that could have appeared to influence the work reported in this paper.

Acknowledgments

The first author is grateful for the Foundation for Science and Technology's support through funding UIDB/04625/2020 from the research unit CERIS (DOI: 10.54499/UIDB/04625/2020).

Data availability

Data will be made available on request.

References

Anagnostou, G., Kovári, K., 1994. The face stability of slurry-shield-driven tunnels. Tunn. Undergr. Space Technol. 9 (2), 165–174. http://dx.doi.org/10.1016/0886-7798(94)90028-0, URL http://www.sciencedirect.com/science/article/pii/0886779894900280.

Anagnostou, G., Kovári, K., 1996. Face stability conditions with earth-pressure-balanced shields. Tunn. Undergr. Space Technol. 11 (2), 165–173. http://dx.doi.org/10.1016/0886-7798(96)00017-X, URL http://www.sciencedirect.com/science/article/pii/088677989600017X.

Antão, A.N., 1997. Analyse de la Stabilité des Ouvrages Souterrains par une Méthode Cinématique Régularisée (Ph.D. thesis). L'École Nationale des Ponts et Chaussées, Paris.

Antão, A.N., Santana, T.G., da Silva, M.V., Guerra, N.M., 2016. Three-dimensional active earth pressure coefficients by upper bound numerical limit analysis. Comput. Geotech. 79, 96–104. http://dx.doi.org/10.1016/j.compgeo.2016.05.022, URL http://www.sciencedirect.com/science/article/pii/S0266352X16301227.

Atkinson, J.H., Potts, D.M., 1977. Stability of a shallow circular tunnel in cohesionless soil. Géotechnique 27 (2), 203–215. http://dx.doi.org/10.1680/geot.1977.27.2.203, arXiv:https://doi.org/10.1680/geot.1977.27.2.203.

Atkinson, J.H., Potts, D.M., 1981. Soil mechanics aspects of soft ground tunnelling. Ground Eng..

Chambon, P., Corté, J.-F., 1994. Shallow tunnels in cohesionless soil: Stability of tunnel face. J. Geotech. Eng. 120 (7), 1148–1165. http://dx.doi.org/10.1061/(ASCE)0733-9410(1994)120:7(1148).

Chambon, P., Corté, J.-F., Garnier, J., König, D., 1991. Face stability of shallow tunnels in granular soils. In: Proceeding of the International Conference Centrifuge. Balkema, Rotterdam, pp. 99–106.

Chen, R., Li, J., gang Kong, L., jun Tang, L., 2013. Experimental study on face instability of shield tunnel in sand. Tunn. Undergr. Space Technol. 33, 12–21. http://dx.doi.org/10.1016/j.tust.2012.08.001, URL http://www.sciencedirect.com/science/article/pii/S0886779812001447.

Ellstein, A., 1986. Heading failure of lined tunnels in soft soils. Tunn. Tunn. 18, 51–54.

Griffiths, D.V., Huang, J., 2009. Observations on the extended Matsuoka-Nakai failure criterion. Int. J. Numer. Anal. Methods Geomech. 33 (17), 1889–1905. http://dx.doi.org/10.1002/nag.810, arXiv:https://onlinelibrary.wiley.com/doi/pdf/10.1002/nag.810 URL https://onlinelibrary.wiley.com/doi/abs/10.1002/nag.810.

Horn, M., 1961. Horizontaler erddruck auf senkrechte abschluß flächen von tunnelröhren. In: Landeskonferenz des Ungarischen Tiefbauindustrie. STUVA Dusseldorf German traduction.

Janssen, H.A., 1895. Versuche über getreidedruck in silozeilen. Z. Vereins Dtsch. Ing. XXXIX (35), 1045–1049.

Kirsch, A., 2010. Experimental investigation of the face stability of shallow tunnels in sand. Acta Geotech. 5 (1), 43–62. http://dx.doi.org/10.1007/s11440-010-0110-7.

König, D., Güttler, U., Jessberger, 1991. Stress redistributions during tunnel and shaft constructions. In: Proceeding of the International Conference Centrifuge. Balkema, Rotterdam, pp. 128–135.

Leca, E., Dormieux, L., 1990. Upper and lower bound solutions for the face stability of shallow circular tunnels in frictional material. Géotechnique 40 (4), 581–606. http://dx.doi.org/10.1680/geot.1990.40.4.581, arXiv:http://dx.doi.org/10.1680/geot.1990.40.4.581.

Leca, E., Panet, M., 1988. Application du calcul à la rupture à la stabilité du front de taille d'un tunnel. Rev. Française Géotech. 43, 5–19..

Martin, C.M., 2011. The use of adaptive finite-element limit analysis to reveal slip-line fields. Géotech. Lett. 1 (2), 23–29.

Matsuoka, H., Nakai, T., 1974. Stress-deformation and strength characteristics of soil under three different principal stresses. Proc. Jpn. Soc. Civ. Eng. 1974 (232), 59–70. http://dx.doi.org/10.2208/jscej1969.1974.232_59.

Matsuoka, H., Nakai, T., 1985. Relationship among tresca, mises, Mohr-Coulomb and Matsuoka-Nakai failure criteria. Soils Found. 25 (4), 123–128. http://dx.doi.org/10.3208/sandf1972.25.4_123.

Mollon, G., Dias, D., Soubra, A.-H., 2010. Face stability analysis of circular tunnels driven by a pressurized shield. J. Geotech. Geoenviron. Eng. 136 (1), http://dx.doi.org/10.1061/(ASCE)GT.1943-5606.0000194, URL http://ascelibrary.org/doi/abs/10.1061/%28ASCE%29GT.1943-5606.0000194.

Mollon, G., Dias, D., Soubra, A.-H., 2011. Rotational failure mechanisms for the face stability analysis of tunnels driven by a pressurized shield. Int. J. Numer. Anal. Methods Geomech. 35 (12), 1363–1388. http://dx.doi.org/10.1002/nag.962.

Mühlhaus, H.-B., 1985. Lower bound solutions for circular tunnels in two and three dimensions. Rock Mech. Rock Eng. 18 (1), 37–52. http://dx.doi.org/10.1007/BF01020414.

Proctor, R.V., White, T.L., 1977. Earth Tunneling with Steel Supports. Comercial Shearing, Inc., Youngstown, Ohio..

Santana, T., Antão, A., Guerra, N., Vicente da Silva, M., 2023. Upper bounds for the three-dimensional seismic active earth pressure coefficients. Géotech. Lett. 13 (1), 1–10. http://dx.doi.org/10.1680/jgele.22.00096, arXiv:https://doi.org/10.1680/jgele.22.00096.

Shiau, J., Al-Asadi, F., 2020. Determination of critical tunnel heading pressures using stability factors. Comput. Geotech. 119, 103345. http://dx.doi.org/10.1016/j.compgeo.2019.103345, URL http://www.sciencedirect.com/science/article/pii/S0266352X19304094.

Subrin, D., Wong, H., 2002. Stabilité du front d'un tunnel en milieu frottant : un nouveau mécanisme de rupture 3D. C. R. Méc. 330 (7), 513–519. http://dx.doi.org/10.1016/S1631-0721(02)01491-2, URL http://www.sciencedirect.com/science/article/pii/S1631072102014912.

Terzaghi, K., 1943. Theoretical Soil Mechanics. John Wiley & Sons, INC,.

Vicente da Silva, M., Antão, A., 2023a. Mechpy's webpage. http://http://geocluster.dec.fct.unl.pt/mechpy. (Accessed 26 September 2023).

Vicente da Silva, M., Antão, A., 2023b. Three-dimensional limit analysis using the Extended-Matsuoka–Nakai yield criterion. Comput. Geotech. 161, 105526. http://dx.doi.org/10.1016/j.compgeo.2023.105526, URL https://www.sciencedirect.com/science/article/pii/S0266352X23002835.

Vicente da Silva, M., Deusdado, N., Antão, A., 2020. Lower and upper bound limit analysis via the alternating direction method of multipliers. Comput. Geotech. 124, 103571. http://dx.doi.org/10.1016/j.compgeo.2020.103571, URL http://www.sciencedirect.com/science/article/pii/S0266352X20301348.

Zhang, X., Wang, M., Li, J., Wang, Z., Tong, J., Liu, D., 2020. Safety factor analysis of a tunnel face with an unsupported span in cohesive-frictional soils. Comput. Geotech. 117, 103221. http://dx.doi.org/10.1016/j.compgeo.2019.103221, URL http://www.sciencedirect.com/science/article/pii/S0266352X1930285X.